Challenges and opportunities of three-photon tomographic reconstruction for the XEnon Medical Imaging System

Workshop EmiLy 2022

07/11/2022

Mehdi Latif[1,2], Jérôme Idier[1], Thomas Carlier[2], Simon Stute[2]

[1] SiMS,LS2N - Ecole Centrale Nantes,
[2] Nuclear Oncology, CRCI2NA - CHU de Nantes

Table of contents

Table of contents

XEnon Medical Imaging System (XEMIS)

Project start-up: 2004 by XENON team - SUBATECH laboratory (France).

XEnon Medical Imaging System (XEMIS)

Project start-up: 2004 by XENON team - SUBATECH laboratory (France).

XEMIS - Grignon et al. [2007]

Low-activity medical imaging

Development of the Compton camera with liquid xenon (LXe);

XEnon Medical Imaging System (XEMIS)

Project start-up: 2004 by XENON team - SUBATECH laboratory (France).

XEMIS - Grignon et al. [2007]

Low-activity medical imaging

- Development of the Compton camera with liquid xenon (LXe);
- Based on the three-photon imaging technique (3γ)

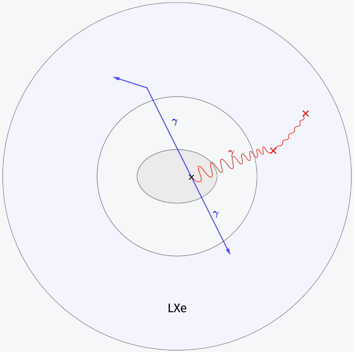

3γ imaging technique in XEMIS LXe detector.

Project start-up: 2004 by XENON team - SUBATECH laboratory (France).

XEMIS - Grignon et al. [2007]

Low-activity medical imaging

- Development of the Compton camera with liquid xenon (LXe);
- Based on the three-photon imaging technique (3γ)

Three-phased project:

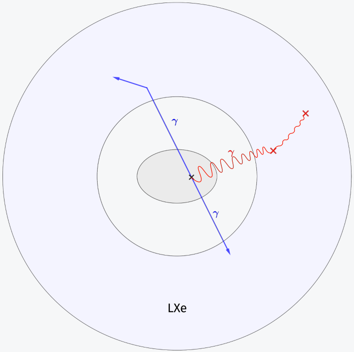

3γ imaging technique in XEMIS LXe detector.

Project start-up: 2004 by XENON team - SUBATECH laboratory (France).

XEMIS - Grignon et al. [2007]

Low-activity medical imaging

- Development of the Compton camera with liquid xenon (LXe);
- Based on the three-photon imaging technique (3γ)

Three-phased project:

- **XEMIS1:** Development of the LXe Compton telescope prototype;

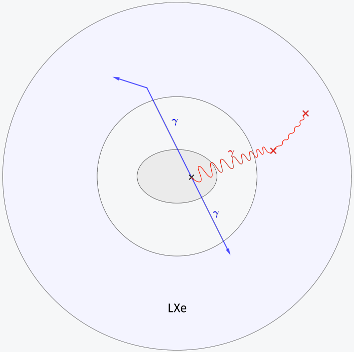

3γ imaging technique in XEMIS LXe detector.

Project start-up: 2004 by XENON team - SUBATECH laboratory (France).

XEMIS - Grignon et al. [2007]

Low-activity medical imaging

- Development of the Compton camera with liquid xenon (LXe);
- Based on the three-photon imaging technique (3γ)

Three-phased project:

- **XEMIS1:** Development of the LXe Compton telescope prototype;
- **XEMIS2:** LXe pre-clinical camera for rodents total-body imaging;

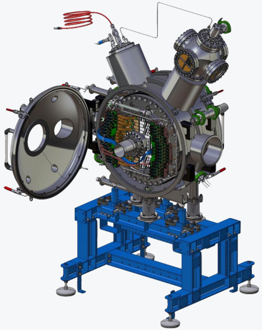

XEMIS2 sketch[1]

[1] **Source:** SUBATECH laboratory.

XEnon Medical Imaging System (XEMIS)

Project start-up: 2004 by XENON team - SUBATECH laboratory (France).

XEMIS - Grignon et al. [2007]

Low-activity medical imaging

- Development of the Compton camera with liquid xenon (LXe);
- Based on the three-photon imaging technique (3γ)

Three-phased project:

- **XEMIS1:** Development of the LXe Compton telescope prototype;
- **XEMIS2:** LXe pre-clinical camera for rodents total-body imaging;

XEMIS2 camera - CHU-CIMA Nantes[1]

[1] **Source:** SUBATECH laboratory.

XEnon Medical Imaging System (XEMIS)

Project start-up: 2004 by XENON team - SUBATECH laboratory (France).

XEMIS - Grignon et al. [2007]

Low-activity medical imaging

- Development of the Compton camera with liquid xenon (LXe);
- Based on the three-photon imaging technique (3γ)

Three-phased project:

- **XEMIS1:** Development of the LXe Compton telescope prototype;
- **XEMIS2:** LXe pre-clinical camera for rodents total-body imaging;
- **XEMIS3:** LXe clinical camera for total-body imaging.

XEMIS2 camera - CHU-CIMA Nantes[1]

[1] **Source:** SUBATECH laboratory.

XEnon Medical Imaging System (XEMIS)

Project start-up: 2004 by XENON team - SUBATECH laboratory (France).

XEMIS - Grignon et al. [2007]

Low-activity medical imaging

- Development of the Compton camera with liquid xenon (LXe);
- Based on the three-photon imaging technique (3γ)

Three-phased project:

- **XEMIS1:** Development of the LXe Compton telescope prototype;
- **XEMIS2:** LXe pre-clinical camera for rodents total-body imaging;
- **XEMIS3:** LXe clinical camera for total-body imaging.

XEMIS2 camera - CHU-CIMA Nantes[1]

Efforts are spent in **experimental design** of the camera.

[1] **Source:** SUBATECH laboratory.

Table of contents

Statistical model

Notations: $I := \#(\text{LOR})$, $J := \#(\text{voxels})$, $B := \#(\text{TOF-bins})$.

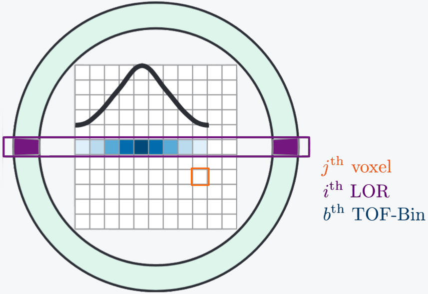

Notations - Cherry et al. [2012]

Statistical model

Notations: $I := \#(\text{LOR})$, $J := \#(\text{voxels})$, $B := \#(\text{TOF-bins})$.

Tomographic reconstruction $\equiv$ inverse problem

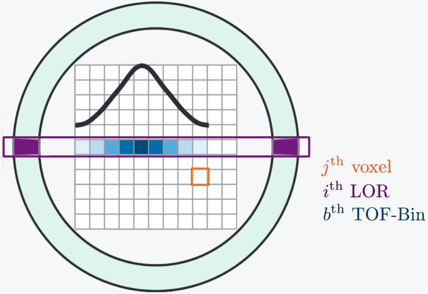

Notations - Cherry et al. [2012]

Statistical model

Notations: $I := \#(\text{LOR})$, $J := \#(\text{voxels})$, $B := \#(\text{TOF-bins})$.

Tomographic reconstruction $\equiv$ inverse problem

Given the measured coincidences: $\boldsymbol{y} := (y_{ib})_{i \in [\![1,I]\!], b \in [\![1,B]\!]}$;

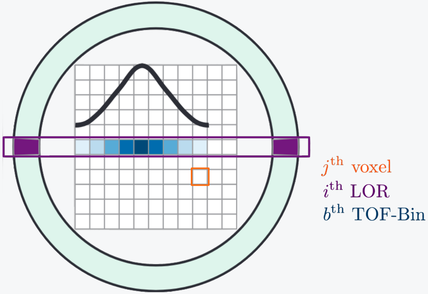

Notations - Cherry et al. [2012]

Notations: $I := \#(\text{LOR})$, $J := \#(\text{voxels})$, $B := \#(\text{TOF-bins})$.

Tomographic reconstruction $\equiv$ inverse problem

Given the measured coincidences: $\boldsymbol{y} := (y_{ib})_{i\in[\![1,I]\!],b\in[\![1,B]\!]}$;

Estimate the radioactive density: $\boldsymbol{\lambda} := (\lambda_j)_{j\in[\![1,J]\!]}$.

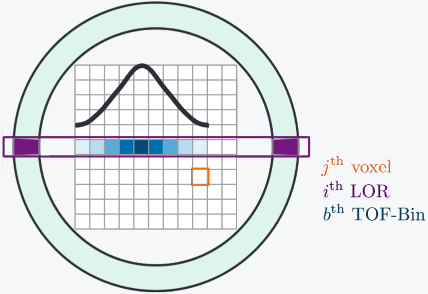

Notations - Cherry et al. [2012]

Notations: $I := \#(\text{LOR})$, $J := \#(\text{voxels})$, $B := \#(\text{TOF-bins})$.

Tomographic reconstruction $\equiv$ inverse problem

Given the measured coincidences: $\boldsymbol{y} := (y_{ib})_{i\in[\![1,I]\!],b\in[\![1,B]\!]}$;

Estimate the radioactive density: $\boldsymbol{\lambda} := (\lambda_j)_{j\in[\![1,J]\!]}$.

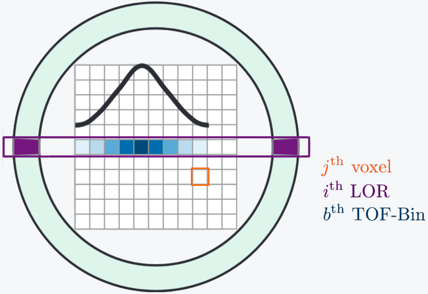

Notations - Cherry et al. [2012]

Direct model

y_{ib} are i.i.d. s.t.

$$y_{ib} \sim \mathcal{P}(\overline{y}_{ib}) \quad \forall i \in [\![1, I]\!], \quad \forall b \in [\![1, B]\!]$$

Statistical model

Notations: $I := \#(\text{LOR})$, $J := \#(\text{voxels})$, $B := \#(\text{TOF-bins})$.

Tomographic reconstruction $\equiv$ inverse problem

Given the measured coincidences: $\boldsymbol{y} := (y_{ib})_{i \in [\![1,I]\!], b \in [\![1,B]\!]}$;

Estimate the radioactive density: $\boldsymbol{\lambda} := (\lambda_j)_{j \in [\![1,J]\!]}$.

Direct model

y_{ib} are i.i.d. s.t.

$$y_{ib} \sim \mathcal{P}\left(\overline{y}_{ib}\right) \quad \forall i \in [\![1, I]\!], \quad \forall b \in [\![1, B]\!]$$

$$\overline{y}_{ib} := \sum_{j \in [\![1,J]\!]} A_{ibj} \lambda_j + \overline{s}_{ib} + \overline{r}_i$$

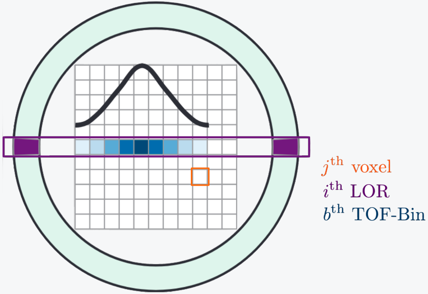

Notations - Cherry et al. [2012]

Notations: $I := \#(\text{LOR})$, $J := \#(\text{voxels})$, $B := \#(\text{TOF-bins})$.

Tomographic reconstruction ≡ inverse problem

Given the measured coincidences: $\boldsymbol{y} := (y_{ib})_{i\in[\![1,I]\!],b\in[\![1,B]\!]}$;

Estimate the radioactive density: $\boldsymbol{\lambda} := (\lambda_j)_{j\in[\![1,J]\!]}$.

Direct model

y_{ib} are i.i.d. s.t.

$$y_{ib} \sim \mathcal{P}(\overline{y}_{ib}) \quad \forall i \in [\![1, I]\!], \quad \forall b \in [\![1, B]\!]$$

$$\overline{y}_{ib} := \sum_{j\in[\![1,J]\!]} A_{ibj}\lambda_j + \overline{s}_{ib} + \overline{r}_i$$

Complex problem

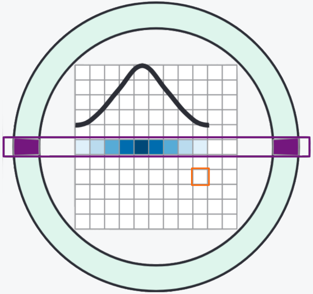

Notations - Cherry et al. [2012]

Notations: $I := \#(\text{LOR})$, $J := \#(\text{voxels})$, $B := \#(\text{TOF-bins})$.

Tomographic reconstruction $\equiv$ inverse problem

Given the measured coincidences: $\boldsymbol{y} := (y_{ib})_{i \in [\![1,I]\!], b \in [\![1,B]\!]}$;

Estimate the radioactive density: $\boldsymbol{\lambda} := (\lambda_j)_{j \in [\![1,J]\!]}$.

Direct model

y_{ib} are i.i.d. s.t.

$$y_{ib} \sim \mathcal{P}(\overline{y}_{ib}) \quad \forall i \in [\![1, I]\!], \quad \forall b \in [\![1, B]\!]$$

$$\overline{y}_{ib} := \sum_{j \in [\![1,J]\!]} A_{ibj} \lambda_j + \overline{s}_{ib} + \overline{r}_i$$

Complex problem

$\Rightarrow$ Large dimensions of $\mathbf{A}$;

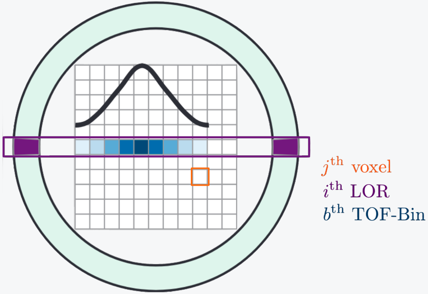

Notations - Cherry et al. [2012]

Statistical model

Notations: $I := \#(\text{LOR})$, $J := \#(\text{voxels})$, $B := \#(\text{TOF-bins})$.

Tomographic reconstruction $\equiv$ inverse problem

Given the measured coincidences: $\boldsymbol{y} := (y_{ib})_{i \in [\![1,I]\!], b \in [\![1,B]\!]}$;

Estimate the radioactive density: $\boldsymbol{\lambda} := (\lambda_j)_{j \in [\![1,J]\!]}$.

Direct model

y_{ib} are i.i.d. s.t.

$$y_{ib} \sim \mathcal{P}\left(\overline{y}_{ib}\right) \quad \forall i \in [\![1, I]\!], \quad \forall b \in [\![1, B]\!]$$

$$\overline{y}_{ib} := \sum_{j \in [\![1,J]\!]} A_{ibj}\lambda_j + \overline{s}_{ib} + \overline{r}_i$$

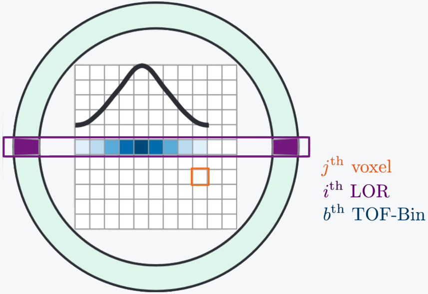

Notations - Cherry et al. [2012]

Complex problem

$\Rightarrow$ Large dimensions of $\mathbf{A}$;

$\Rightarrow$ Noisy measurement vector $\boldsymbol{y}$;

Statistical model

Notations: $I := \#(\text{LOR})$, $J := \#(\text{voxels})$, $B := \#(\text{TOF-bins})$.

Tomographic reconstruction $\equiv$ inverse problem

Given the measured coincidences: $\boldsymbol{y} := (y_{ib})_{i\in[\![1,I]\!],b\in[\![1,B]\!]}$;

Estimate the radioactive density: $\boldsymbol{\lambda} := (\lambda_j)_{j\in[\![1,J]\!]}$.

Direct model

y_{ib} are i.i.d. s.t.

$$y_{ib} \sim \mathcal{P}(\overline{y}_{ib}) \quad \forall i \in [\![1, I]\!], \quad \forall b \in [\![1, B]\!]$$

$$\overline{y}_{ib} := \sum_{j\in[\![1,J]\!]} A_{ibj}\lambda_j + \overline{s}_{ib} + \overline{r}_i$$

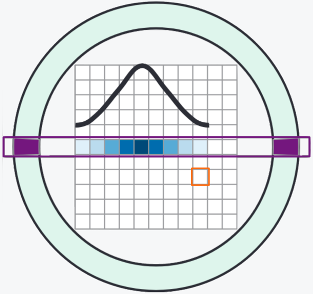

Notations - Cherry et al. [2012]

Complex problem

$\Rightarrow$ Large dimensions of $\mathbf{A}$;

$\Rightarrow$ Noisy measurement vector $\boldsymbol{y}$;

$\Rightarrow$ Small perturbation in projection space $\rightsquigarrow$ Large error in image space.

Maximum-Likelihood Expectation-Maximization for PET -Vardi et al. [1985], Lange et al. [1984]

$$\widehat{\boldsymbol{\lambda}}^{\mathrm{ML}} = \underset{\boldsymbol{\lambda} \in \mathbb{R}_+^J}{\mathbf{argmax}} \left(\log(\mathcal{L}(\boldsymbol{\lambda} | \boldsymbol{y})) \right)$$

Maximum-Likelihood Expectation-Maximization for PET -Vardi et al. [1985], Lange et al. [1984]

$$\widehat{\boldsymbol{\lambda}}^{\mathrm{ML}} = \underset{\boldsymbol{\lambda}\in\mathbb{R}_+^J}{\mathbf{argmax}} \left(\log(\mathcal{L}(\boldsymbol{\lambda}|\boldsymbol{y}))\right)$$

MLEM algorithm[1]:

Determine $\widehat{\boldsymbol{\lambda}}^{\mathrm{ML}}$ for a probabilistic model depending on latent data;

[1] Originally developed by Dempster et al. [1977].

Maximum-Likelihood Expectation-Maximization for PET -Vardi et al. [1985], Lange et al. [1984]

$$\widehat{\boldsymbol{\lambda}}^{\mathrm{ML}} = \underset{\boldsymbol{\lambda}\in\mathbb{R}_+^J}{\mathbf{argmax}} \left(\log(\mathcal{L}(\boldsymbol{\lambda}|\boldsymbol{y}))\right)$$

MLEM algorithm[1]:

Determine $\widehat{\boldsymbol{\lambda}}^{\mathrm{ML}}$ for a probabilistic model depending on latent data;

Likelihood update equations:

$$\begin{cases} \boldsymbol{\lambda}^{(\mathbf{0})} &= \lambda_j^{(0)} > 0 \\ \lambda_j^{(t+1)} &= \lambda_j^{(t)} \times \dfrac{1}{\sum\limits_{\substack{i\in[\![1,I]\!]\\ b\in[\![1,B]\!]}} A_{ibj}} \sum\limits_{\substack{i\in[\![1,I]\!]\\ b\in[\![1,B]\!]}} A_{ibj} \dfrac{y_{ib}}{\sum\limits_{j'\in[\![1,J]\!]} A_{ibj'}\lambda_{j'}^{(t)} + \overline{s}_{ib} + \overline{r}_i} \quad \forall j \in [\![1, J]\!] \end{cases}$$

[1] Originally developed by Dempster et al. [1977].

Maximum-Likelihood Expectation-Maximization for PET -Vardi et al. [1985], Lange et al. [1984]

$$\widehat{\boldsymbol{\lambda}}^{\mathrm{ML}} = \underset{\boldsymbol{\lambda} \in \mathbb{R}_+^J}{\mathbf{argmax}} \left(\log(\mathcal{L}(\boldsymbol{\lambda}|\boldsymbol{y}))\right)$$

MLEM algorithm[1]:

Determine $\widehat{\boldsymbol{\lambda}}^{\mathrm{ML}}$ for a probabilistic model depending on latent data;

Likelihood update equations:

$$\begin{cases} \boldsymbol{\lambda}^{(\mathbf{0})} & = & \lambda_j^{(0)} > 0 \\ \lambda_j^{(t+1)} & = & \lambda_j^{(t)} \times \dfrac{1}{\sum\limits_{\substack{i \in [\![1,I]\!] \\ b \in [\![1,B]\!]}} A_{ibj}} \sum\limits_{\substack{i \in [\![1,I]\!] \\ b \in [\![1,B]\!]}} A_{ibj} \dfrac{y_{ib}}{\sum\limits_{j' \in [\![1,J]\!]} A_{ibj'} \lambda_{j'}^{(t)} + \bar{s}_{ib} + \bar{r}_i} \quad \forall j \in [\![1, J]\!] \end{cases}$$

Properties:

- The MLEM converges to a $\widehat{\boldsymbol{\lambda}}^{\mathrm{ML}}$;
- The densities (λ_j) are non-negative.

[1] Originally developed by Dempster et al. [1977].

List-Mode MLEM - Parra and Barrett [1998]

$$\widehat{\boldsymbol{\lambda}}^{\mathrm{ML}} = \underset{\boldsymbol{\lambda} \in \mathbb{R}_+^J}{\mathbf{argmax}} \left(\log(\mathcal{L}(\boldsymbol{\lambda}|\boldsymbol{y})) \right)$$

List-Mode MLEM - Parra and Barrett [1998]

$$\widehat{\boldsymbol{\lambda}}^{\mathrm{ML}} = \underset{\boldsymbol{\lambda} \in \mathbb{R}_+^J}{\mathbf{argmax}} \left(\log(\mathcal{L}(\boldsymbol{\lambda}|\boldsymbol{y})) \right)$$

LM-MLEM algorithm:

Determine $\widehat{\boldsymbol{\lambda}}^{\mathrm{ML}}$ for a model depending on **latent data** with the **only detected events**[1] stored in a **list** L;

[1] Spatial, temporal and energy data.

List-Mode MLEM - Parra and Barrett [1998]

$$\widehat{\boldsymbol{\lambda}}^{\mathrm{ML}} = \underset{\boldsymbol{\lambda} \in \mathbb{R}_+^J}{\mathbf{argmax}} \left(\log(\mathcal{L}(\boldsymbol{\lambda}|\boldsymbol{y})) \right)$$

LM-MLEM algorithm:

Determine $\widehat{\boldsymbol{\lambda}}^{\mathrm{ML}}$ for a model depending on **latent data** with the **only detected events**[1] stored in a **list** L;

Likelihood update equations:

$$\begin{cases} \boldsymbol{\lambda}^{(\mathbf{0})} & = \lambda_j^{(0)} > 0 \\ \lambda_j^{(t+1)} & = \lambda_j^{(t)} \times \dfrac{1}{\sum\limits_{\substack{i \in [\![1,I]\!] \\ b \in [\![1,B]\!]}} A_{ibj}} \sum\limits_{n \in [\![1,N]\!]} A_{i_n b_n j} \dfrac{1}{\sum\limits_{j' \in [\![1,J]\!]} A_{i_n b_n j'} \lambda_{j'}^{(t)} + \bar{s}_{i_n b_n} + \bar{r}_{i_n}} \quad \forall j \in [\![1, J]\!] \end{cases}$$

where $y_{ib} \in \{0, 1\}$ $\forall i \in [\![1, I]\!], b \in [\![1, B]\!]$ and $N := \mathbf{Card}(L)$

[1] Spatial, temporal and energy data.

List-Mode MLEM - Parra and Barrett [1998]

$$\widehat{\boldsymbol{\lambda}}^{\mathrm{ML}} = \underset{\boldsymbol{\lambda}\in\mathbb{R}_+^J}{\mathbf{argmax}} \left(\log(\mathcal{L}(\boldsymbol{\lambda}|\boldsymbol{y}))\right)$$

LM-MLEM algorithm:

Determine $\widehat{\boldsymbol{\lambda}}^{\mathrm{ML}}$ for a model depending on **latent data** with the **only detected events**[1] stored in a **list** L;

Likelihood update equations:

$$\begin{cases} \boldsymbol{\lambda}^{(\mathbf{0})} & = & \lambda_j^{(0)} > 0 \\ \lambda_j^{(t+1)} & = & \lambda_j^{(t)} \times \dfrac{1}{\sum\limits_{\substack{i\in[\![1,I]\!]\\ b\in[\![1,B]\!]}} A_{ibj}} \sum\limits_{n\in[\![1,N]\!]} A_{i_n b_n j} \dfrac{1}{\sum\limits_{j'\in[\![1,J]\!]} A_{i_n b_n j'} \lambda_{j'}^{(t)} + \overline{s}_{i_n b_n} + \overline{r}_{i_n}} \quad \forall j \in [\![1, J]\!] \end{cases}$$

where $y_{ib} \in \{0, 1\}$ $\forall i \in [\![1, I]\!], b \in [\![1, B]\!]$ and $N := \mathbf{Card}(L)$

Further properties:

- Each event can be treated as a point in a continuous measurement space;

$\Rightarrow$ **No discretization** of data $\rightsquigarrow$ preserve accuracy of measurement.

[1] Spatial, temporal and energy data.

List-Mode MLEM - Parra and Barrett [1998]

$$\widehat{\boldsymbol{\lambda}}^{\mathrm{ML}} = \underset{\boldsymbol{\lambda}\in\mathbb{R}_+^J}{\mathbf{argmax}}\left(\log(\mathcal{L}(\boldsymbol{\lambda}|\boldsymbol{y}))\right)$$

LM-MLEM algorithm:

Determine $\widehat{\boldsymbol{\lambda}}^{\mathrm{ML}}$ for a model depending on **latent data** with the **only detected events**[1] stored in a **list** L;

Likelihood update equations:

$$\begin{cases} \boldsymbol{\lambda}^{(\mathbf{0})} & = & \lambda_j^{(0)} > 0 \\ \lambda_j^{(t+1)} & = & \lambda_j^{(t)} \times \dfrac{1}{\sum\limits_{i\in[\![1,I]\!]} \int A_{ij}(v)\mathrm{d}v} \sum\limits_{n\in[\![1,N]\!]} A_{i_n j}(v_n) \dfrac{1}{\sum\limits_{j'\in[\![1,J]\!]} A_{i_n j'}(v_n)\lambda_{j'}^{(t)} + \bar{s}_{i_n}(v_n) + \bar{r}_{i_n}} \quad \forall j \in [\![1,J]\!] \end{cases}$$

where $y_{ib} \in \{0,1\}\ \forall i \in [\![1,I]\!], b \in [\![1,B]\!]$ and $N := \mathbf{Card}(L)$

Further properties:

- Each event can be treated as a point in a continuous measurement space;

$\Rightarrow$ **No discretization** of data $\rightsquigarrow$ preserve accuracy of measurement.

[1] Spatial, temporal and energy data.

Table of contents

XEMIS2 camera & 3γ imaging

XEMIS2

A monolithic, cylindrical & total-body Compton camera:

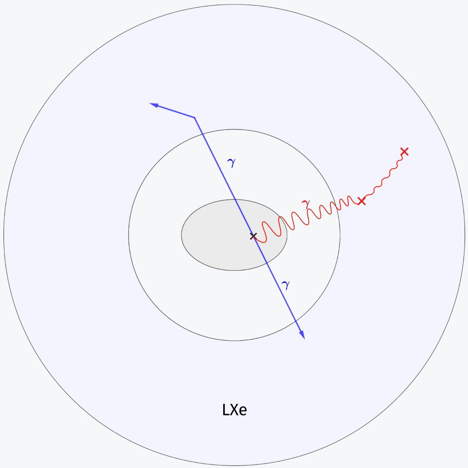

LXe active zone: 24cm in length, 7cm (resp. 19cm) of inner (resp. outer) radius.

XEMIS2 camera & 3γ imaging

XEMIS2

A monolithic, cylindrical & total-body Compton camera:

Scandium-44: (β^+, γ) radionuclide:

$$\begin{aligned} {}^{44}_{21}\mathrm{Sc} &\xrightarrow[94.27\%]{\beta^+} {}^{44}_{20}\mathrm{Ca}^* + \nu_e + e^+ \\ {}^{44}_{20}\mathrm{Ca}^* &\xrightarrow{\gamma} {}^{44}_{20}\mathrm{Ca} + \gamma \end{aligned} \quad \text{with } E_0 = 1.157\mathrm{MeV}.$$

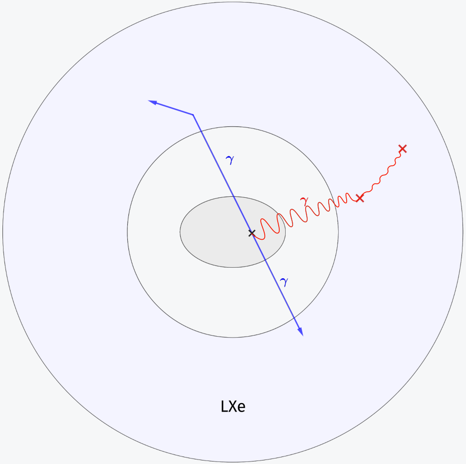

LXe active zone: 24cm in length, 7cm (resp. 19cm) of inner (resp. outer) radius.

XEMIS2

A monolithic, cylindrical & total-body Compton camera:

Scandium-44: (β^+, γ) radionuclide:

$$ {}^{44}_{21}\mathrm{Sc} \xrightarrow[94.27\%]{\beta^+} {}^{44}_{20}\mathrm{Ca}^* + \nu_e + e^+ $$

$$ {}^{44}_{20}\mathrm{Ca}^* \xrightarrow{\gamma} {}^{44}_{20}\mathrm{Ca} + \gamma $$

with $E_0 = 1.157\mathrm{MeV}$.

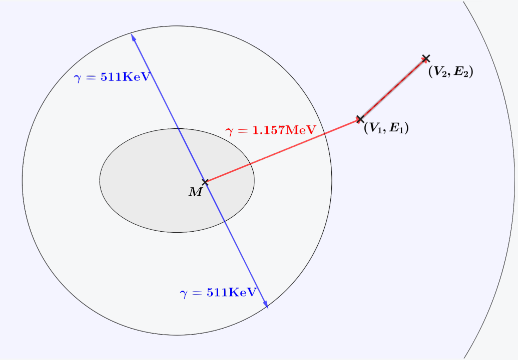

Assumptions

Let M be a decay source

XEMIS2

A monolithic, cylindrical & total-body Compton camera:

Scandium-44: (β^+, γ) radionuclide:

$$\begin{aligned} {}^{44}_{21}\mathrm{Sc} &\xrightarrow[94.27\%]{\beta^+} {}^{44}_{20}\mathrm{Ca}^* + \nu_e + e^+ \\ {}^{44}_{20}\mathrm{Ca}^* &\xrightarrow{\gamma} {}^{44}_{20}\mathrm{Ca} + \gamma \end{aligned} \quad \text{with } E_0 = 1.157\mathrm{MeV}.$$

Assumptions

Let M be a decay source $\Rightarrow$ **Compton cone**:

Apex: V_1;

Axis: $\Delta = \overrightarrow{V_2 V_1}$;

Angle: $\theta = \arccos\left(1 - \frac{m_e c^2 E_1}{E_0(E_0 - E_1)}\right)$;

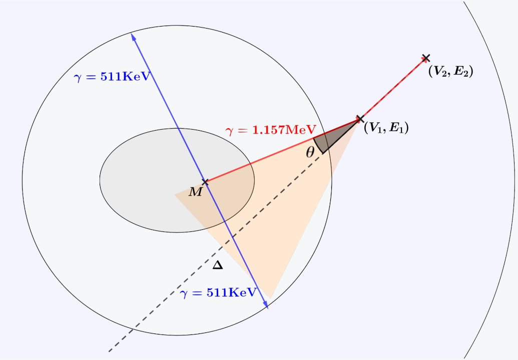

XEMIS2

A monolithic, cylindrical & total-body Compton camera:

Scandium-44: (β^+, γ) radionuclide:

$$^{44}_{21}\mathrm{Sc} \xrightarrow[94.27\%]{\beta^+} {}^{44}_{20}\mathrm{Ca}^* + \nu_e + e^+$$

$$^{44}_{20}\mathrm{Ca}^* \xrightarrow{\gamma} {}^{44}_{20}\mathrm{Ca} + \gamma$$

with $E_0 = 1.157\mathrm{MeV}.$

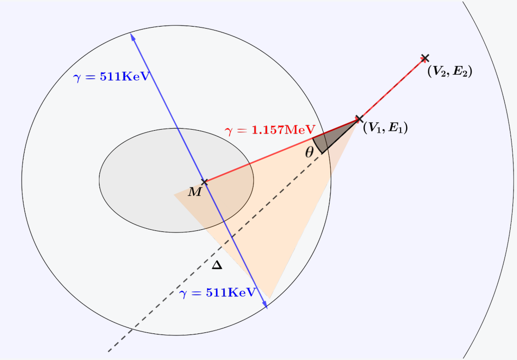

Assumptions

Let M be a decay source $\Rightarrow$ **Compton cone**:

Apex: V_1;

Axis: $\Delta = \overrightarrow{V_2V_1}$;

Angle: $\theta = \arccos\left(1 - \frac{m_e c^2 E_1}{E_0(E_0 - E_1)}\right)$;

Property: M lies on the **Cone-Surface Response** (CSR).

XEMIS2

A monolithic, cylindrical & total-body Compton camera:

Scandium-44: (β^+, γ) radionuclide:

$$
\begin{aligned}
{}^{44}_{21}\mathrm{Sc} &\xrightarrow[94.27\%]{\beta^+} {}^{44}_{20}\mathrm{Ca}^* + \nu_e + e^+ \\
{}^{44}_{20}\mathrm{Ca}^* &\xrightarrow{\gamma} {}^{44}_{20}\mathrm{Ca} + \gamma
\end{aligned}
\quad \text{with } E_0 = 1.157\text{MeV}.
$$

Assumptions

Let M be a decay source $\Rightarrow$ **Compton cone**:

Apex: V_1;

Axis: $\Delta = \overrightarrow{V_2V_1}$;

Angle: $\theta = \arccos\left(1 - \frac{m_e c^2 E_1}{E_0(E_0 - E_1)}\right)$;

Property: M lies on the **Cone-Surface Response** (CSR).

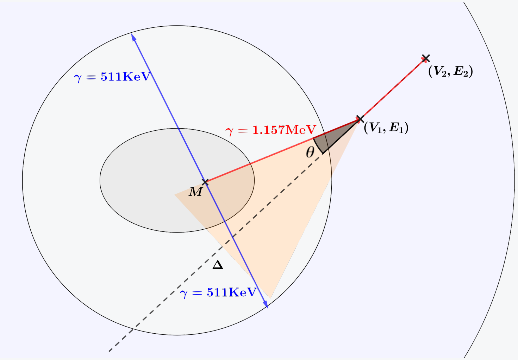

Opportunity: LOR/CSR intersection;

XEMIS2 camera & 3γ imaging

XEMIS2

A monolithic, cylindrical & total-body Compton camera:

Scandium-44: (β^+, γ) radionuclide:

$$^{44}_{21}\mathrm{Sc} \xrightarrow[94.27\%]{\beta^+} {}^{44}_{20}\mathrm{Ca}^* + \nu_e + e^+$$

$$^{44}_{20}\mathrm{Ca}^* \xrightarrow{\gamma} {}^{44}_{20}\mathrm{Ca} + \gamma$$

with $E_0 = 1.157\mathrm{MeV}.$

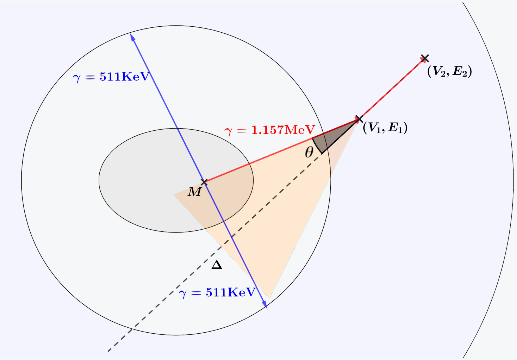

Assumptions

Let M be a decay source $\Rightarrow$ **Compton cone**:

Apex: V_1;

Axis: $\Delta = \overrightarrow{V_2V_1}$;

Angle: $\theta = \arccos\left(1 - \frac{m_e c^2 E_1}{E_0(E_0 - E_1)}\right)$;

Property: M lies on the **Cone-Surface Response** (CSR).

Opportunity: LOR/CSR intersection;

Challenge: Reconstruct the image from a continuous 3γ signal.

State of the art: Image Reconstruction for 3γ PET Imaging - Giovagnoli et al. [2021]

Idea: continuous 3γ reconstruction as **TOF-PET** using block detectors.

Idea: continuous 3γ reconstruction as **TOF-PET** using block detectors.

Pseudo-TOF method:

Transform information from 3rd γ into a TOF information $\Rightarrow \mathcal{N}(v, \sigma^2)$

v **:** LOR/CSR Intersection (LCI);

σ **:** pseudo-TOF standard deviation.

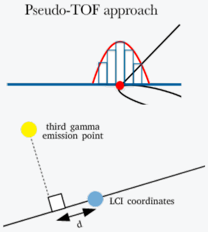

Pseudo-TOF Method[1]

[1] **Source:** Giovagnoli [2020]

Idea: continuous 3γ reconstruction as **TOF-PET** using block detectors.

Pseudo-TOF method:

Transform information from 3rd γ into a TOF information $\Rightarrow \mathcal{N}(v, \sigma^2)$

v : LOR/CSR Intersection (LCI);

σ : pseudo-TOF standard deviation.

Assumptions :

- σ is **fixed** whatever the orientation of the γ wrt. the LOR;

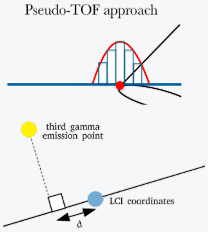

Pseudo-TOF Method[1]

[1] **Source:** Giovagnoli [2020]

Idea: continuous 3γ reconstruction as **TOF-PET** using block detectors.

Pseudo-TOF method:

Transform information from 3rd γ into a TOF information $\Rightarrow \mathcal{N}(v, \sigma^2)$

v : LOR/CSR Intersection (LCI);

σ : pseudo-TOF standard deviation.

Assumptions :

- σ is **fixed** whatever the orientation of the γ wrt. the LOR;
- **Virtual** discretization of the continuous detector;

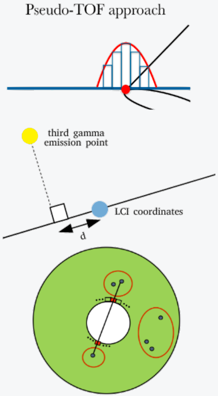

Pseudo-TOF Method[1]

[1] **Source:** Giovagnoli [2020]

Idea: continuous 3γ reconstruction as **TOF-PET** using block detectors.

Pseudo-TOF method:

Transform information from 3rd γ into a TOF information $\Rightarrow \mathcal{N}(v, \sigma^2)$

v : LOR/CSR Intersection (LCI);

σ : pseudo-TOF standard deviation.

Assumptions :

- σ is **fixed** whatever the orientation of the γ wrt. the LOR;
- **Virtual** discretization of the continuous detector;
- **Only** 3γ **events** are taken into account.

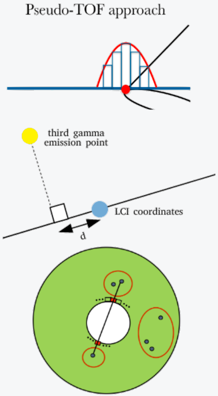

Pseudo-TOF Method[1]

[1] **Source:** Giovagnoli [2020]

Idea: continuous 3γ reconstruction as **TOF-PET** using block detectors.

Pseudo-TOF method:

Transform information from 3rd γ into a TOF information $\Rightarrow \mathcal{N}(v, \sigma^2)$

v **:** LOR/CSR Intersection (LCI);

σ **:** pseudo-TOF standard deviation.

Assumptions :

- σ is **fixed** whatever the orientation of the γ wrt. the LOR;
- **Virtual** discretization of the continuous detector;
- **Only** 3γ **events** are taken into account.

Proportions of events:

$$\boxed{\mathbf{3\gamma \quad \sim 10\%}}, 2\gamma \quad \sim 50\%, 1\gamma \quad \sim 40\%$$

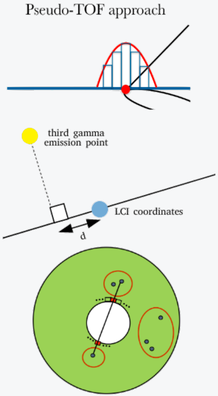

Pseudo-TOF Method[1]

[1] **Source:** Giovagnoli [2020]

Table of contents

Our approach

$$\boxed{\mathbf{3\gamma \quad \sim 10\%}},\quad 2\gamma \quad \sim 50\%,\ 1\gamma \quad \sim 40\%$$

Our approach

$$\boxed{\mathbf{3}\gamma \ \sim \mathbf{10\%},\ \ \mathbf{2}\gamma \ \sim \mathbf{50\%},\ \mathbf{1}\gamma \ \sim \mathbf{40\%}}$$

Our approach

$$\boxed{\mathbf{3\gamma} \ \sim \mathbf{10\%},\ \ \mathbf{2\gamma} \ \sim \mathbf{50\%},\ \mathbf{1\gamma} \ \sim \mathbf{40\%}}$$

Purpose of my PhD thesis

Design and **implementation** of reconstruction algorithms for the 3γ imaging provided by the XEMIS2 camera.

Our approach

$$\boxed{\mathbf{3}\boldsymbol{\gamma} \;\; \sim \mathbf{10\%},\;\; \mathbf{2}\boldsymbol{\gamma} \;\; \sim \mathbf{50\%},\; \mathbf{1}\boldsymbol{\gamma} \;\; \sim \mathbf{40\%}}$$

Purpose of my PhD thesis

Design and **implementation** of reconstruction algorithms for the 3γ imaging provided by the XEMIS2 camera.

Our methodology

- Derivation of a LM-MLEM algorithm taking into account

Our approach

$$\boxed{\mathbf{3\gamma} \ \sim \mathbf{10\%}, \ \ \mathbf{2\gamma} \ \sim \mathbf{50\%}, \ \mathbf{1\gamma} \ \sim \mathbf{40\%}}$$

Purpose of my PhD thesis

Design and **implementation** of reconstruction algorithms for the 3γ imaging provided by the XEMIS2 camera.

Our methodology

- Derivation of a LM-MLEM algorithm taking into account
  - the continuous aspect of the LXe detection space

Our approach

$$\boxed{\mathbf{3}\gamma \sim \mathbf{10\%},\ \mathbf{2}\gamma \sim \mathbf{50\%},\ \mathbf{1}\gamma \sim \mathbf{40\%}}$$

Purpose of my PhD thesis

Design and **implementation** of reconstruction algorithms for the 3γ imaging provided by the XEMIS2 camera.

Our methodology

- Derivation of a LM-MLEM algorithm taking into account
  - the continuous aspect of the LXe detection space
  - handling the all types of events i.e. 1γ, 2γ or 3γ

Continuous LM-MLEM

Reformulation of the LM-MLEM in the **continuous space** :

Continuous LM-MLEM

Reformulation of the LM-MLEM in the **continuous space** :

$$\left\{\begin{array}{rcl} \boldsymbol{\lambda}^{(\mathbf{0})} & = & \lambda_j^{(0)} > 0 \\ \lambda_j^{(t+1)} & = & \lambda_j^{(t)} \times \dfrac{1}{\int_{\delta\in\mathcal{L}} A_j(\delta)\mathrm{d}\delta} \displaystyle\sum_{n\in[\![1,N]\!]} A_j(\delta_n) \dfrac{1}{\displaystyle\sum_{j'\in[\![1,J]\!]} A_{j'}(\delta_n)\lambda_{j'}^{(t)} + \varepsilon(\delta_n)} \quad \forall j \in [\![1,J]\!] \end{array}\right.$$

where

δ**:** integration variable associated to an **event**;

Continuous LM-MLEM

Reformulation of the LM-MLEM in the **continuous space** :

$$\left\{\begin{array}{rcl}\boldsymbol{\lambda}^{(0)} & = & \lambda_j^{(0)} > 0 \\ \lambda_j^{(t+1)} & = & \lambda_j^{(t)} \times \dfrac{1}{\int_{\delta \in \mathcal{L}} A_j(\delta) \mathrm{d}\delta} \displaystyle\sum_{n \in [\![1,N]\!]} A_j(\delta_n) \dfrac{1}{\displaystyle\sum_{j' \in [\![1,J]\!]} A_{j'}(\delta_n) \lambda_{j'}^{(t)} + \varepsilon(\delta_n)} \quad \forall j \in [\![1,J]\!] \end{array}\right.$$

where

- δ**:** integration variable associated to an **event**;
- $\mathcal{L}$**:** **detection domain** given by:

Reformulation of the LM-MLEM in the **continuous space** :

$$\begin{cases} \boldsymbol{\lambda}^{(0)} &= \lambda_j^{(0)} > 0 \\ \lambda_j^{(t+1)} &= \lambda_j^{(t)} \times \dfrac{1}{\int_{\delta \in \mathcal{L}} A_j(\delta) \mathrm{d}\delta} \displaystyle\sum_{n \in [\![1,N]\!]} A_j(\delta_n) \dfrac{1}{\displaystyle\sum_{j' \in [\![1,J]\!]} A_{j'}(\delta_n) \lambda_{j'}^{(t)} + \varepsilon(\delta_n)} \quad \forall j \in [\![1,J]\!] \end{cases}$$

where

δ: integration variable associated to an **event**;

$\mathcal{L}$: **detection domain** given by:

1γ: a CSR with $E_0 = 511\mathrm{keV}$
or a CSR with $E_0 = 1.157\mathrm{MeV}$

Continuous LM-MLEM

Reformulation of the LM-MLEM in the **continuous space** :

$$\begin{cases} \boldsymbol{\lambda}^{(0)} & = \lambda_j^{(0)} > 0 \\ \lambda_j^{(t+1)} & = \lambda_j^{(t)} \times \dfrac{1}{\int_{\delta \in \mathcal{L}} A_j(\delta) \mathrm{d}\delta} \displaystyle\sum_{n \in [\![1,N]\!]} A_j(\delta_n) \dfrac{1}{\displaystyle\sum_{j' \in [\![1,J]\!]} A_{j'}(\delta_n) \lambda_{j'}^{(t)} + \varepsilon(\delta_n)} \quad \forall j \in [\![1, J]\!] \end{cases}$$

where

δ: integration variable associated to an **event**;

$\mathcal{L}$: **detection domain** given by:

1γ: a CSR with $E_0 = 511\mathrm{keV}$
or a CSR with $E_0 = 1.157\mathrm{MeV}$

2γ: a LOR i.e. $2 \times E_0 = 511\mathrm{keV}$
or a 2 CSR intersection with $E_0 = 511\mathrm{keV}$ & $E_0 = 1.157\mathrm{MeV}$

Continuous LM-MLEM

Reformulation of the LM-MLEM in the **continuous space** :

$$\begin{cases} \boldsymbol{\lambda^{(0)}} & = & \lambda_j^{(0)} > 0 \\ \lambda_j^{(t+1)} & = & \lambda_j^{(t)} \times \dfrac{1}{\int_{\delta \in \mathcal{L}} A_j(\delta) \mathrm{d}\delta} \sum_{n \in [\![1,N]\!]} A_j(\delta_n) \dfrac{1}{\sum_{j' \in [\![1,J]\!]} A_{j'}(\delta_n) \lambda_{j'}^{(t)} + \varepsilon(\delta_n)} \quad \forall j \in [\![1,J]\!] \end{cases}$$

where

δ**:** integration variable associated to an **event**;

$\mathcal{L}$**:** **detection domain** given by:

1γ**:** a CSR with $E_0 = 511\text{keV}$
or a CSR with $E_0 = 1.157\text{MeV}$

2γ**:** a LOR i.e. $2 \times E_0 = 511\text{keV}$
or a 2 CSR intersection with $E_0 = 511\text{keV}$ & $E_0 = 1.157\text{MeV}$

3γ**:** a combination of independent LOR & CSR.

Reformulation of the LM-MLEM in the **continuous space** :

$$\left\{ \begin{array}{rcl} \boldsymbol{\lambda}^{(0)} & = & \lambda_j^{(0)} > 0 \\ \lambda_j^{(t+1)} & = & \lambda_j^{(t)} \times \dfrac{1}{\int_{\delta \in \mathcal{L}} A_j(\delta) \mathrm{d}\delta} \displaystyle\sum_{n \in [\![1,N]\!]} A_j(\delta_n) \dfrac{1}{\displaystyle\sum_{j' \in [\![1,J]\!]} A_{j'}(\delta_n) \lambda_{j'}^{(t)} + \varepsilon(\delta_n)} \quad \forall j \in [\![1,J]\!] \end{array} \right.$$

where

δ: integration variable associated to an **event**;

$\mathcal{L}$: **detection domain** given by:

1γ: a CSR with $E_0 = 511\text{keV}$
or a CSR with $E_0 = 1.157\text{MeV}$

2γ: a LOR i.e. $2 \times E_0 = 511\text{keV}$
or a 2 CSR intersection with $E_0 = 511\text{keV}$ & $E_0 = 1.157\text{MeV}$

3γ: a combination of independent LOR & CSR.

So: there are 5 types of events to consider!

Reformulation of the LM-MLEM in the **continuous space** :

$$\begin{cases} \boldsymbol{\lambda}^{(0)} & = \quad \lambda_j^{(0)} > 0 \\ \lambda_j^{(t+1)} & = \quad \lambda_j^{(t)} \times \underbrace{\frac{1}{\int_{\delta \in \mathcal{L}} A_j(\delta) \mathrm{d}\delta}}_{=s_j} \sum_{n \in [\![1,N]\!]} A_j(\delta_n) \frac{1}{\sum_{j' \in [\![1,J]\!]} A_{j'}(\delta_n) \lambda_{j'}^{(t)} + \varepsilon(\delta_n)} \quad \forall j \in [\![1,J]\!] \end{cases}$$

where

δ: integration variable associated to an **event**;

$\mathcal{L}$: **detection domain** given by:

- 1γ: a CSR with $E_0 = 511\text{keV}$
  or a CSR with $E_0 = 1.157\text{MeV}$
- 2γ: a LOR i.e. $2 \times E_0 = 511\text{keV}$
  or a 2 CSR intersection with $E_0 = 511\text{keV}$ & $E_0 = 1.157\text{MeV}$
- 3γ: a combination of independent LOR & CSR.

So: there are 5 types of events to consider!

Inspiration: Maxim et al. [2015], Feng [2019] for LM-MLEM Compton reconstruction.

Let M be an emission point of a E_0 photon belonging to the voxel j in the FOV

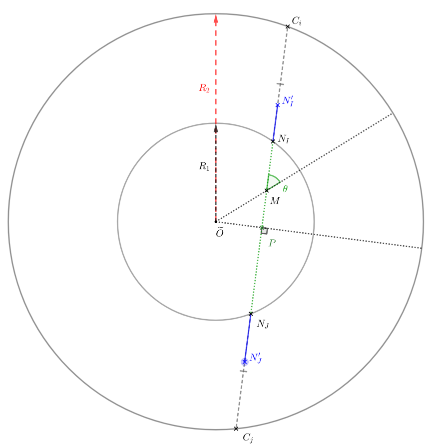

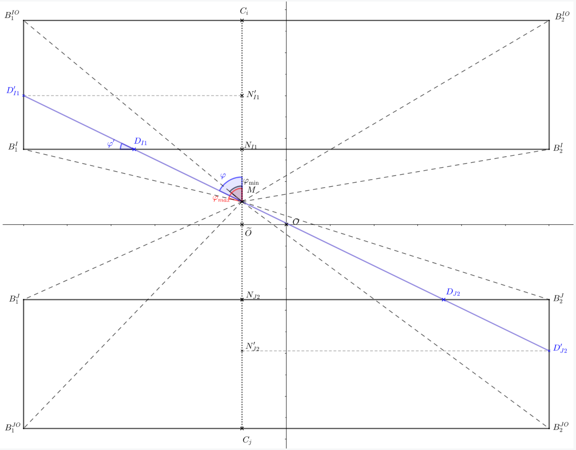

2γ Annihilation case

Inspiration: Maxim et al. [2015], Feng [2019] for LM-MLEM Compton reconstruction.

Let M be an emission point of a E_0 photon belonging to the voxel j in the FOV

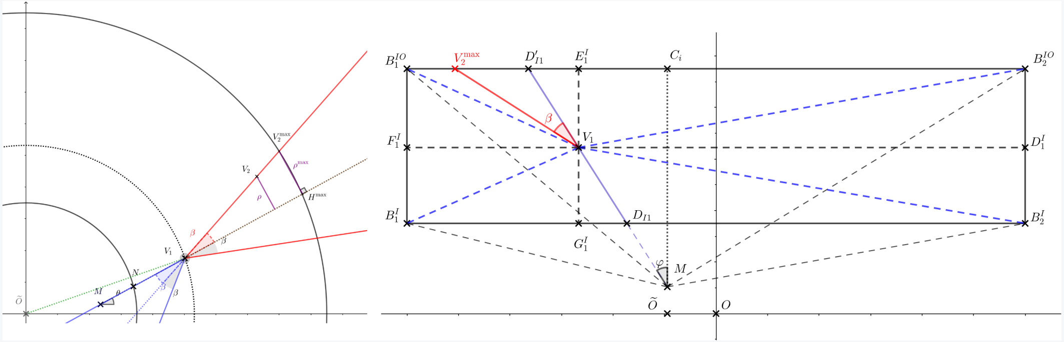

1γ case with incident energy E_0

Sensitivity calculation

Let M be an emission point of a E_0 photon belonging to the voxel j in the FOV:

$$s_{2\gamma}(M) := \int_{\theta=0}^{\pi}\int_{\varphi=0}^{\frac{\pi}{2}} p_i\left(\frac{1}{|\cos(\varphi)|}\left(\sqrt{R_{\text{out}}^{2\gamma}(\varphi, I1)^2 - \widetilde{O\,P}^2} - Q\right)\right) \times p_i\left(\frac{1}{|\cos(\varphi)|}\left(\sqrt{R_{\text{out}}^{2\gamma}(\varphi, J2)^2 - \widetilde{O\,P}^2} - Q\right)\right)\mathrm{d}\varphi$$

$$+ \int_{\varphi=-\frac{\pi}{2}}^{0} p_i\left(\frac{1}{|\cos(\varphi)|}\left(\sqrt{R_{\text{out}}^{2\gamma}(\varphi, I2)^2 - \widetilde{O\,P}^2} - Q\right)\right) \times p_i\left(\frac{1}{|\cos(\varphi)|}\left(\sqrt{R_{\text{out}}^{2\gamma}(\varphi, J1)^2 - \widetilde{O\,P}^2} - Q\right)\right)\mathrm{d}\varphi\mathrm{d}\theta$$

$$\widetilde{O\,P} := \sin(\theta)\,\widetilde{O\,M}, \quad Q := \sqrt{R_1^2 - \widetilde{O\,P}^2}.$$

$$s_{1\gamma}(M) := \int_{\theta=0}^{2\pi}\left[\int_{\varphi=0}^{\frac{\pi}{2}}\int_{v=R_{\text{in}}}^{R_{\text{out}}^{1\gamma}(\varphi, I1)} h(\varphi,\theta,v)\mathrm{d}v\mathrm{d}\varphi + \int_{\varphi=\frac{\pi}{2}}^{\pi}\int_{v=R_{\text{in}}}^{R_{\text{out}}^{1\gamma}(\varphi, J1)} h(\varphi,\theta,v)\mathrm{d}v\mathrm{d}\varphi\right.$$

$$\left. + \int_{\varphi=-\frac{\pi}{2}}^{0}\int_{v=R_{\text{in}}}^{R_{\text{out}}^{1\gamma}(\varphi, I2)} h(\varphi,\theta,v)\mathrm{d}v\mathrm{d}\varphi + \int_{\varphi=-\pi}^{-\frac{\pi}{2}}\int_{v=R_{\text{in}}}^{R_{\text{out}}^{1\gamma}(\varphi, J2)} h(\varphi,\theta,v)\mathrm{d}v\mathrm{d}\varphi\right]\mathrm{d}\theta$$

$$\text{with } h(\varphi,\theta,v) := f(\varphi,\theta,v) \times C(v,\theta,\varphi)$$

$$f(\varphi,\theta,v) := p_i\left(\frac{1}{|\cos(\varphi)|}\left(\sqrt{v^2 - \sin^2(\theta)\,\widetilde{O\,M}^2} - \sqrt{R_{\text{in}}^2 - \sin^2(\theta)\,\widetilde{O\,M}^2}\right)\right)$$

$$C(v,\theta,\varphi) := \int_{\beta=-\pi}^{\pi} K(\beta|E_0)\int_{\omega=0}^{2\pi}\int_{\rho=0}^{\rho_{\max}(v,\theta,\varphi,\beta,\omega)} p_i'\left(\|\overrightarrow{V_1V_2}\|_2\right)\mathrm{d}\beta\mathrm{d}\omega\mathrm{d}\rho$$

Algorithm implementation: using CASToR[1] framework - Merlin et al. [2018];

[1] Customizable and Advanced Software for Tomographic Reconstruction

Algorithm implementation: using CASToR[1] framework - Merlin et al. [2018];

For the time being

CASToR is implemented for **standard PET camera**:

[1] Customizable and Advanced Software for Tomographic Reconstruction

Algorithm implementation: using CASToR[1] framework - Merlin et al. [2018];

For the time being

CASToR is implemented for **standard PET camera**:

- discrete detectors;

[1] Customizable and Advanced Software for Tomographic Reconstruction

Algorithm implementation: using CASToR[1] framework - Merlin et al. [2018];

For the time being

CASToR is implemented for **standard PET camera**:

- discrete detectors;
- LOR events.

[1] Customizable and Advanced Software for Tomographic Reconstruction

Algorithm implementation: using CASToR[1] framework - Merlin et al. [2018];

For the time being

CASToR is implemented for **standard PET camera**:

- discrete detectors;
- LOR events.

Upgrading Castor

We have to **extend** CASToR with:

[1] Customizable and Advanced Software for Tomographic Reconstruction

Algorithm implementation: using CASToR[1] framework - Merlin et al. [2018];

For the time being

CASToR is implemented for **standard PET camera**:

- discrete detectors;
- LOR events.

Upgrading Castor

We have to **extend** CASToR with:

- continuous detection space capability with associated sensitivity computation;

[1] Customizable and Advanced Software for Tomographic Reconstruction

Algorithm implementation: using CASToR[1] framework - Merlin et al. [2018];

For the time being

CASToR is implemented for **standard PET camera**:

- discrete detectors;
- LOR events.

Upgrading Castor

We have to **extend** CASToR with:

- continuous detection space capability with associated sensitivity computation;
- a CSR projector *e.g.* Ellipse-stacking method or Ray-tracing method[2];

[1] Customizable and Advanced Software for Tomographic Reconstruction

[2] **Sources:** Ellipse-stacking method - Wilderman et al. [1998], Ray-tracing method - Kim et al. [2007]

Algorithm implementation: using CASToR[1] framework - Merlin et al. [2018];

For the time being

CASToR is implemented for **standard PET camera**:

- discrete detectors;
- LOR events.

Upgrading Castor

We have to **extend** CASToR with:

- continuous detection space capability with associated sensitivity computation;
- a CSR projector *e.g.* Ellipse-stacking method or Ray-tracing method[2];
- new types of events including 1γ for Compton imaging and 3γ.

[1] Customizable and Advanced Software for Tomographic Reconstruction

[2] **Sources:** Ellipse-stacking method - Wilderman et al. [1998], Ray-tracing method - Kim et al. [2007]

Algorithm implementation: using CASToR[1] framework - Merlin et al. [2018];

For the time being

CASToR is implemented for **standard PET camera**:

- discrete detectors;
- LOR events.

Upgrading Castor

We have to **extend** CASToR with:

- continuous detection space capability with associated sensitivity computation;
- a CSR projector *e.g.* Ellipse-stacking method or Ray-tracing method[2];
- new types of events including 1γ for Compton imaging and 3γ.

$\Rightarrow$ Some data are required!

[1] Customizable and Advanced Software for Tomographic Reconstruction

[2] **Sources:** Ellipse-stacking method - Wilderman et al. [1998], Ray-tracing method - Kim et al. [2007]

Algorithm implementation: using CASToR[1] framework - Merlin et al. [2018];

For the time being

CASToR is implemented for **standard PET camera**:

- discrete detectors;
- LOR events.

Upgrading Castor

We have to **extend** CASToR with:

- continuous detection space capability with associated sensitivity computation;
- a CSR projector *e.g.* Ellipse-stacking method or Ray-tracing method[2];
- new types of events including 1γ for Compton imaging and 3γ.

$\Rightarrow$ Some data are required!

Hello POLLUX!

A simple **home-made** Monte Carlo simulator based on **ray-tracing** techniques with some physical considerations *e.g.* positron range, mean free path, photon cross section, ...

[1] Customizable and Advanced Software for Tomographic Reconstruction

[2] **Sources:** Ellipse-stacking method - Wilderman et al. [1998], Ray-tracing method - Kim et al. [2007]

POLLUX - 2γ LOR case

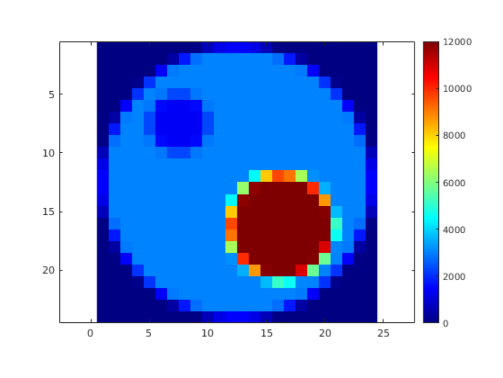

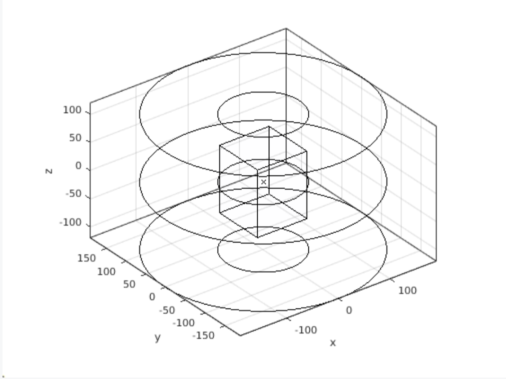

Voxel size: $4 \times 4 \times 4 \text{ mm}^3$

Image size: $96 \times 96 \times 120 \text{ mm}^3$

Total number of voxel: $J = 17280$

LXe active zone:

- 24cm in length;
- 7cm (resp. 19cm) of inner (resp. outer) radius.

POLLUX - 2γ LOR case

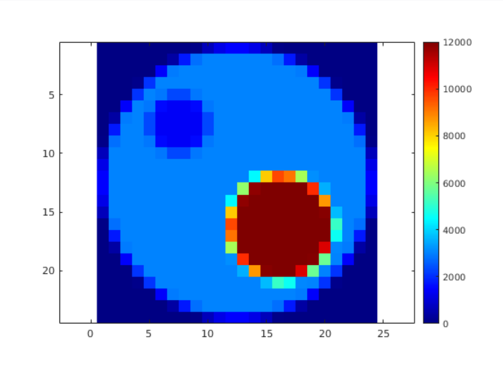

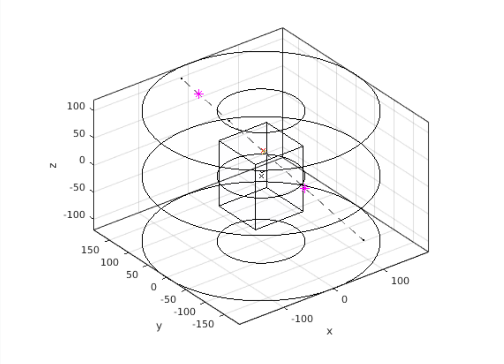

Voxel size: $4 \times 4 \times 4$ mm^3

Image size: $96 \times 96 \times 120$ mm^3

Total number of voxel: $J = 17280$

Positron range: $\sim \mathcal{N}(\mu, 2)$ with $\mu = 2.4$ [1];

LXe Density: $\rho \approx 3.06$ g.cm^{-3};

Attenuation coeff.: $\mu \approx 0.291$ cm^{-1} at $511\mathrm{keV}$.

[1] Source: Giovagnoli et al. [2021]

POLLUX - 2γ LOR case

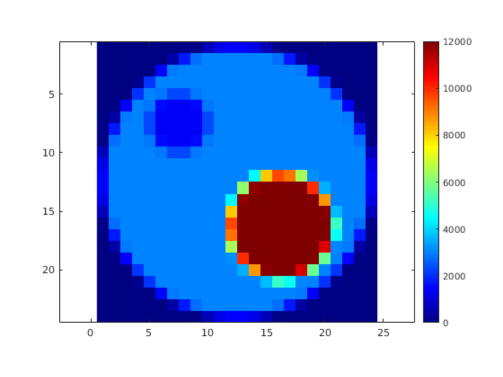

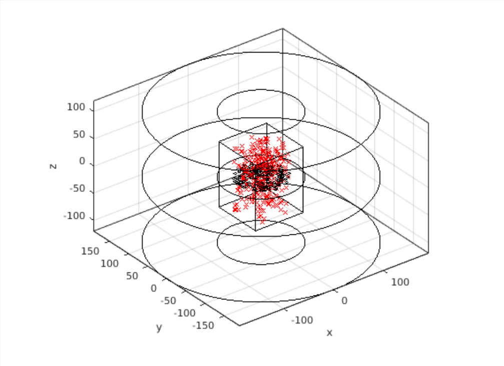

Voxel size: $4 \times 4 \times 4$ mm^3

Image size: $96 \times 96 \times 120$ mm^3

Total number of voxel: $J = 17280$

Repeat N times *e.g.* $N = 200$

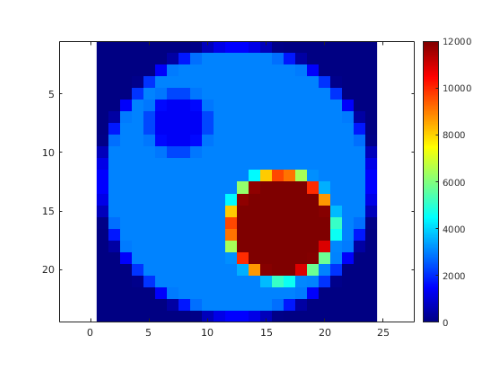

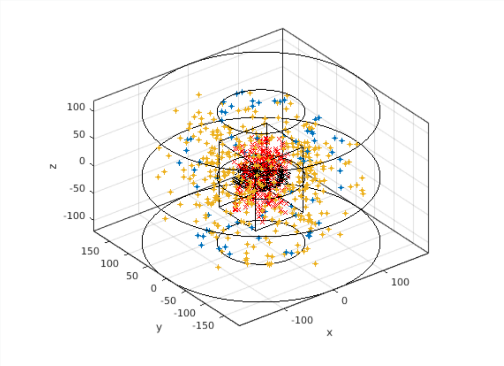

Voxel size: $4 \times 4 \times 4\ \text{mm}^3$

Image size: $96 \times 96 \times 120\ \text{mm}^3$

Total number of voxel: $J = 17280$

POLLUX - 2γ LOR case

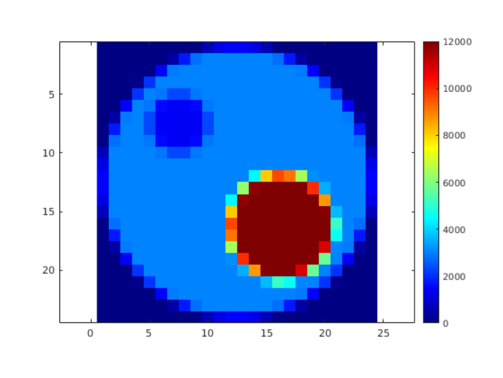

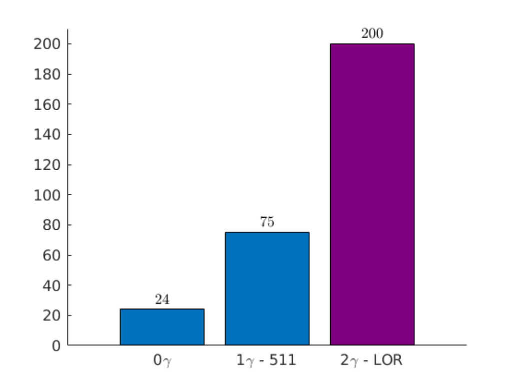

Voxel size: $4 \times 4 \times 4$ mm^3

Image size: $96 \times 96 \times 120$ mm^3

Total number of voxel: $J = 17280$

Table of contents

Next steps:

Sensitivity calculation:

$\Rightarrow$ Evaluation of the multiples integrals with Monte Carlo calculation implemented in CASToR.

Next steps:

Sensitivity calculation:

$\Rightarrow$ Evaluation of the multiples integrals with Monte Carlo calculation implemented in CASToR.

Continuous LM-MLEM :

Consider the 5 types of events in the reconstruction method;

Next steps:

Sensitivity calculation:

$\Rightarrow$ Evaluation of the multiples integrals with Monte Carlo calculation implemented in CASToR.

Continuous LM-MLEM :

Consider the 5 types of events in the reconstruction method;

$\Rightarrow$ Derivation of the maximum likelihood equation for the cases $1, 2, 3\gamma$;

Next steps:

Sensitivity calculation:

$\Rightarrow$ Evaluation of the multiples integrals with Monte Carlo calculation implemented in CASToR.

Continuous LM-MLEM :

Consider the 5 types of events in the reconstruction method;

$\Rightarrow$ Derivation of the maximum likelihood equation for the cases $1, 2, 3\gamma$;

Design of the dedicated algorithm and implementation in **CASToR** framework;

Next steps:

Sensitivity calculation:

$\Rightarrow$ Evaluation of the multiples integrals with Monte Carlo calculation implemented in CASToR.

Continuous LM-MLEM :

Consider the 5 types of events in the reconstruction method;

$\Rightarrow$ Derivation of the maximum likelihood equation for the cases $1, 2, 3\gamma$;

Design of the dedicated algorithm and implementation in **CASToR** framework;

Assessment of the algorithm with simulated[1] and real data.

[1] *e.g.* with GATE simulation platform - Jan et al. [2004]

Thank you for your attention

Questions?

References i

Cherry, S. R., Sorenson, J. A., and Phelps, M. E. (2012). Physics in nuclear medicine e-Book. Elsevier Health Sciences.

Dempster, A. P., Laird, N. M., and Rubin, D. B. (1977). Maximum likelihood from incomplete data via the em algorithm. Journal of the Royal Statistical Society. Series B (Methodological), 39(1):1–38.

Feng, Y. (2019). Modeling and regularization in tomographic reconstruction for Compton camera imaging. Theses, Université de Lyon.

Giovagnoli, D. (2020). Image reconstruction for three-gamma PET imaging. Theses, Ecole nationale supérieure Mines-Télécom Atlantique.

Giovagnoli, D., Bousse, A., Beaupere, N., Canot, C., Cussonneau, J.-P., Diglio, S., Iborra Carreres, A., Masbou, J., Merlin, T., Morteau, E., Xing, Y., Zhu, Y., Thers, D., and Visvikis, D. (2021). A pseudo-tof image reconstruction approach for three-gamma small animal imaging. IEEE Transactions on Radiation and Plasma Medical Sciences, 5(6):826–834.

Grignon, C., Barbet, J., Bardiès, M., Carlier, T., Chatal, J., Couturier, O., Cussonneau, J., Faivre, A., Ferrer, L., Girault, S., Haruyama, T., Le Ray, P., Luquin, L., Lupone, S., Métivier, V., Morteau, E., Servagent, N., and Thers, D. (2007). Nuclear medical imaging using $\beta+\gamma$ coincidences from 44sc radio-nuclide with liquid xenon as detection medium. Nuclear Instruments and Methods in Physics Research Section A: Accelerators, Spectrometers, Detectors and Associated Equipment, 571(1):142–145. Proceedings of the 1st International Conference on Molecular Imaging Technology.

Jan, S., Santin, G., Strul, D., Staelens, S., Assié, K., Autret, D., Avner, S., Barbier, R., Bardiès, M., Bloomfield, P. M., Brasse, D., Breton, V., Bruyndonckx, P., Buvat, I., Chatziioannou, A. F., Choi, Y., Chung, Y. H., Comtat, C., Donnarieix, D., Ferrer, L., Glick, S. J., Groiselle, C. J., Guez, D., Honore, P.-F., Kerhoas-Cavata, S., Kirov, A. S., Kohli, V., Koole, M., Krieguer, M., van der Laan, D. J., Lamare, F., Largeron, G., Lartizien, C., Lazaro, D., Maas, M. C., Maigne, L., Mayet, F., Melot, F., Merheb, C., Pennacchio, E., Perez, J., Pietrzyk, U., Rannou, F. R., Rey, M., Schaart, D. R., Schmidtlein, C. R., Simon, L., Song, T. Y., Vieira, J.-M., Visvikis, D., de Walle, R. V., Wieërs, E., and Morel, C. (2004). Gate: a simulation toolkit for pet and spect. Physics in Medicine & Biology, 49(19):4543.

Kim, S. M., Lee, J. S., Lee, M. N., Lee, J. H., Lee, C. S., Kim, C.-H., Lee, D. S., and Lee, S.-J. (2007). Two approaches to implementing projector–backprojector pairs for 3d reconstruction from compton scattered data. Nuclear Instruments and Methods in Physics Research Section A: Accelerators, Spectrometers, Detectors and Associated Equipment, 571(1):255–258. Proceedings of the 1st International Conference on Molecular Imaging Technology.

Lange, K., Carson, R., and Carson, R. (1984). EM reconstruction algorithms for emission and transmission tomography. Journal of Computer Assisted Tomography, 8(2):306–316.

Maxim, V., Lojacono, X., Hilaire, E., Krimmer, J., Testa, E., Dauvergne, D., Magnin, I., and Prost, R. (2015). Probabilistic models and numerical calculation of system matrix and sensitivity in list-mode MLEM 3d reconstruction of compton camera images. Physics in Medicine and Biology, 61(1):243–264.

Merlin, T., Stute, S., Benoit, D., Bert, J., Carlier, T., Comtat, C., Filipovic, M., Lamare, F., and VISVIKIS, D. (2018). CASToR: a generic data organization and processing code framework for multi-modal and multi-dimensional tomographic reconstruction. Physics in Medicine and Biology, 63(18):185005.

Parra, L. C. and Barrett, H. H. (1998). List-mode likelihood: Em algorithm and image quality estimation demonstrated on 2-d pet. IEEE Transactions on Medical Imaging, 17:228–235.

Vardi, Y., Shepp, L. A., and Kaufman, L. (1985). A statistical model for positron emission tomography. Journal of the American Statistical Association, 80(389):8–20.

Wilderman, S., Rogers, W., Knoll, G., and Engdahl, J. (1998). Fast algorithm for list mode back-projection of compton scatter camera data. IEEE Transactions on Nuclear Science, 45(3):957–962.

XEnon Medical Imaging System (XEMIS)

Project start-up: 2004 by XENON team - SUBATECH laboratory (France).

XEMIS - Grignon et al. [2007]

Low-activity medical imaging

- Development of the Compton camera with liquid xenon (LXe);
- Based on the three-photon imaging technique (3γ)

Three-phased project:

- **XEMIS1:** Development of the LXe Compton telescope prototype;
- **XEMIS2:** LXe pre-clinical camera for rodents total-body imaging;
- **XEMIS3:** LXe clinical camera for total-body imaging.

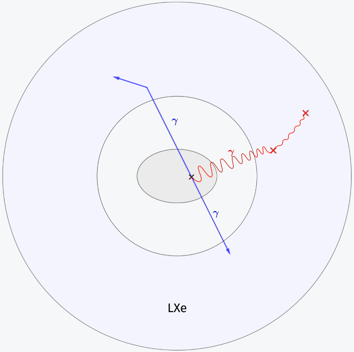

3γ imaging technique in XEMIS LXe detector.

Efforts are spent in **experimental design** of the camera.

[1] **Source:** SUBATECH laboratory.

Statistical model

Notations: $I := \#(\text{LOR})$, $J := \#(\text{voxels})$, $B := \#(\text{TOF-bins})$.

Tomographic reconstruction $\equiv$ inverse problem

Given the measured coincidences: $\boldsymbol{y} := (y_{ib})_{i\in[\![1,I]\!],b\in[\![1,B]\!]}$;

Estimate the radioactive density: $\boldsymbol{\lambda} := (\lambda_j)_{j\in[\![1,J]\!]}$.

Direct model

y_{ib} are i.i.d. s.t.

$$y_{ib} \sim \mathcal{P}(\overline{y}_{ib}) \quad \forall i \in [\![1,I]\!], \quad \forall b \in [\![1,B]\!]$$

$$\overline{y}_{ib} := \sum_{j\in[\![1,J]\!]} A_{ibj}\lambda_j + \overline{s}_{ib} + \overline{r}_i$$

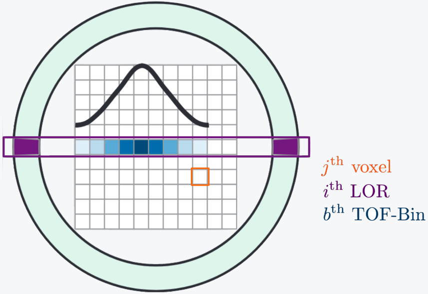

Notations - Cherry et al. [2012]

Complex problem

$\Rightarrow$ Large dimensions of $\mathbf{A}$;

$\Rightarrow$ Noisy measurement vector $\boldsymbol{y}$;

$\Rightarrow$ Small perturbation in projection space $\rightsquigarrow$ Large error in image space.

Maximum-Likelihood Expectation-Maximization for PET -Vardi et al. [1985], Lange et al. [1984]

$$\widehat{\boldsymbol{\lambda}}^{\mathrm{ML}} = \underset{\boldsymbol{\lambda}\in\mathbb{R}_+^J}{\mathbf{argmax}} \left(\log(\mathcal{L}(\boldsymbol{\lambda}|\boldsymbol{y}))\right)$$

MLEM algorithm[1]:

Determine $\widehat{\boldsymbol{\lambda}}^{\mathrm{ML}}$ for a probabilistic model depending on latent data;

Likelihood update equations:

$$\begin{cases} \boldsymbol{\lambda}^{(\mathbf{0})} & = & \lambda_j^{(0)} > 0 \\ \lambda_j^{(t+1)} & = & \lambda_j^{(t)} \times \dfrac{1}{\sum\limits_{\substack{i\in[\![1,I]\!]\\ b\in[\![1,B]\!]}} A_{ibj}} \sum\limits_{\substack{i\in[\![1,I]\!]\\ b\in[\![1,B]\!]}} A_{ibj} \dfrac{y_{ib}}{\sum\limits_{j'\in[\![1,J]\!]} A_{ibj'}\lambda_{j'}^{(t)} + \overline{s}_{ib} + \overline{r}_i} \quad \forall j \in [\![1,J]\!] \\ & & \end{cases}$$

Properties:

- The MLEM converges to a $\widehat{\boldsymbol{\lambda}}^{\mathrm{ML}}$;
- The densities (λ_j) are non-negative.

[1] Originally developed by Dempster et al. [1977].

$$\widehat{\boldsymbol{\lambda}}^{\mathrm{ML}} = \underset{\boldsymbol{\lambda}\in\mathbb{R}_+^J}{\mathbf{argmax}}\left(\log(\mathcal{L}(\boldsymbol{\lambda}|\boldsymbol{y}))\right)$$

LM-MLEM algorithm:

Determine $\widehat{\boldsymbol{\lambda}}^{\mathrm{ML}}$ for a model depending on **latent data** with the **only detected events**[1] stored in a **list** L;

Likelihood update equations:

$$\begin{cases} \boldsymbol{\lambda}^{(\mathbf{0})} = \lambda_j^{(0)} > 0 \\ \lambda_j^{(t+1)} = \lambda_j^{(t)} \times \dfrac{1}{\sum\limits_{i\in[\![1,I]\!]} \int A_{ij}(v)\mathrm{d}v} \sum\limits_{n\in[\![1,N]\!]} A_{i_n j}(v_n) \dfrac{1}{\sum\limits_{j'\in[\![1,J]\!]} A_{i_n j'}(v_n)\lambda_{j'}^{(t)} + \bar{s}_{i_n}(v_n) + \bar{r}_{i_n}} \quad \forall j \in [\![1,J]\!] \end{cases}$$

where $y_{ib} \in \{0,1\}\ \forall i \in [\![1,I]\!], b \in [\![1,B]\!]$ and $N := \mathbf{Card}(L)$

Further properties:

- Each event can be treated as a point in a continuous measurement space;

$\Rightarrow$ **No discretization** of data $\rightsquigarrow$ preserve accuracy of measurement.

[1] Spatial, temporal and energy data.

XEMIS2

A monolithic, cylindrical & total-body Compton camera:

Scandium-44: (β^+, γ) radionuclide:

$$
\begin{aligned}
{}^{44}_{21}\mathrm{Sc} &\xrightarrow[94.27\%]{\beta^+} {}^{44}_{20}\mathrm{Ca}^* + \nu_e + \boldsymbol{e^+} \\
{}^{44}_{20}\mathrm{Ca}^* &\xrightarrow{\gamma} {}^{44}_{20}\mathrm{Ca} + \boldsymbol{\gamma}
\end{aligned}
\qquad \text{with } E_0 = 1.157\mathrm{MeV}.
$$

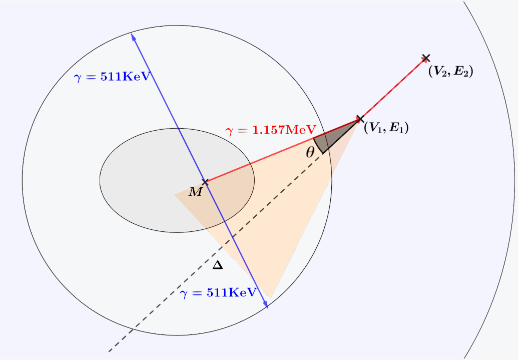

Assumptions

Let M be a decay source $\Rightarrow$ **Compton cone**:

Apex: V_1;

Axis: $\Delta = \overrightarrow{V_2 V_1}$;

Angle: $\theta = \arccos\left(1 - \frac{m_e c^2 E_1}{E_0(E_0 - E_1)}\right)$;

Property: M lies on the **Cone-Surface Response** (CSR).

Opportunity: LOR/CSR intersection;

Challenge: Reconstruct the image from a continuous 3γ signal.

Idea: continuous 3γ reconstruction as **TOF-PET** using block detectors.

Pseudo-TOF method:

Transform information from 3rd γ into a TOF information $\Rightarrow \mathcal{N}(v, \sigma^2)$

v : LOR/CSR Intersection (LCI);

σ : pseudo-TOF standard deviation.

Assumptions :

- σ is **fixed** whatever the orientation of the γ wrt. the LOR;
- **Virtual** discretization of the continuous detector;
- **Only** 3γ **events** are taken into account.

Proportions of events:

$$\boxed{\mathbf{3\gamma \quad \sim 10\%}}, 2\gamma \quad \sim 50\%, 1\gamma \quad \sim 40\%$$

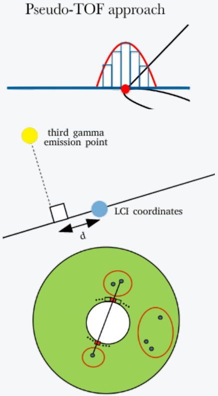

Pseudo-TOF Method[1]

[1] **Source:** Giovagnoli [2020]

Our approach

$$\boxed{\mathbf{3}\gamma \ \sim \mathbf{10\%},\ \ \mathbf{2}\gamma \ \sim \mathbf{50\%},\ \mathbf{1}\gamma \ \sim \mathbf{40\%}}$$

Purpose of my PhD thesis

Design and **implementation** of reconstruction algorithms for the 3γ imaging provided by the XEMIS2 camera.

Our methodology

- Derivation of a LM-MLEM algorithm taking into account
  - the continuous aspect of the LXe detection space
  - handling the all types of events i.e. 1γ, 2γ or 3γ

Continuous LM-MLEM

Reformulation of the LM-MLEM in the **continuous space** :

$$\left\{ \begin{array}{rcl} \boldsymbol{\lambda}^{(0)} & = & \lambda_j^{(0)} > 0 \\ \lambda_j^{(t+1)} & = & \lambda_j^{(t)} \times \underbrace{\frac{1}{\int_{\delta \in \mathcal{L}} A_j(\delta) \mathrm{d}\delta}}_{=s_j} \sum_{n \in [\![1,N]\!]} A_j(\delta_n) \frac{1}{\sum_{j' \in [\![1,J]\!]} A_{j'}(\delta_n) \lambda_{j'}^{(t)} + \varepsilon(\delta_n)} \quad \forall j \in [\![1,J]\!] \end{array} \right.$$

where

δ: integration variable associated to an **event**;

$\mathcal{L}$: **detection domain** given by:

- 1γ: a CSR with $E_0 = 511\text{keV}$
  or a CSR with $E_0 = 1.157\text{MeV}$
- 2γ: a LOR i.e. $2 \times E_0 = 511\text{keV}$
  or a 2 CSR intersection with $E_0 = 511\text{keV}$ & $E_0 = 1.157\text{MeV}$
- 3γ: a combination of independent LOR & CSR.

So: there are 5 types of events to consider!

Algorithm implementation: using CASToR[1] framework - Merlin et al. [2018];

For the time being

CASToR is implemented for **standard PET camera**:

- discrete detectors;
- LOR events.

Upgrading Castor

We have to **extend** CASToR with:

- continuous detection space capability with associated sensitivity computation;
- a CSR projector *e.g.* Ellipse-stacking method or Ray-tracing method[2];
- new types of events including 1γ for Compton imaging and 3γ.

$\Rightarrow$ Some data are required!

Hello POLLUX!

A simple **home-made** Monte Carlo simulator based on **ray-tracing** techniques with some physical considerations *e.g.* positron range, mean free path, photon cross section, ...

[1] Customizable and Advanced Software for Tomographic Reconstruction

[2] **Sources:** Ellipse-stacking method - Wilderman et al. [1998], Ray-tracing method - Kim et al. [2007]

POLLUX - 2γ LOR case

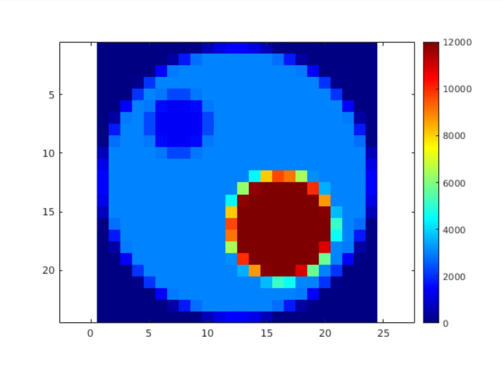

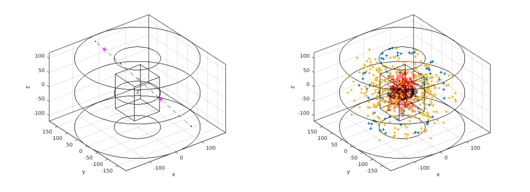

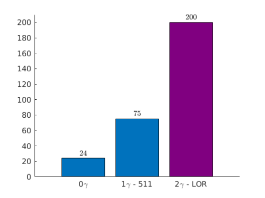

Voxel size: $4 \times 4 \times 4$ mm^3

Image size: $96 \times 96 \times 120$ mm^3

Total number of voxel: $J = 17280$

Positron range: $\sim \mathcal{N}(2.4, 2)$;

LXe Density: $\rho \approx 3.06$ g.cm^{-3};

Attenuation coeff.: $\mu \approx 0.291$ cm^{-1} for $E_0 = 511\mathrm{keV}$.

Next steps:

Sensitivity calculation:

$\Rightarrow$ Evaluation of the multiples integrals with Monte Carlo calculation implemented in CASToR.

Continuous LM-MLEM :

Consider the 5 types of events in the reconstruction method;

$\Rightarrow$ Derivation of the maximum likelihood equation for the cases $1, 2, 3\gamma$;

Design of the dedicated algorithm and implementation in **CASToR** framework;

Assessment of the algorithm with simulated and real data.

Inspiration: Maxim et al. [2015], Feng [2019] for LM-MLEM Compton reconstruction.

Let M be an emission point of a E_0 photon belonging to the voxel j in the FOV

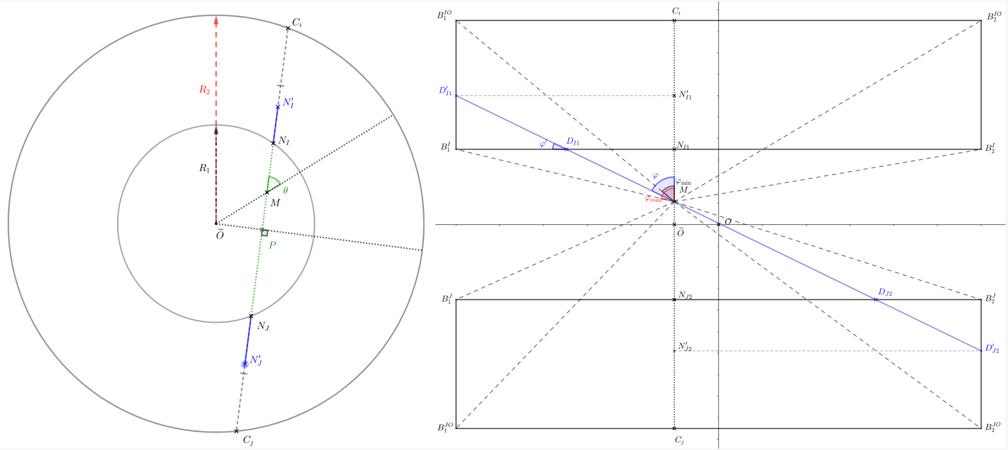

2γ Annihilation case

Sensitivity calculation

Inspiration: Maxim et al. [2015], Feng [2019] for LM-MLEM Compton reconstruction.

Let M be an emission point of a E_0 photon belonging to the voxel j in the FOV

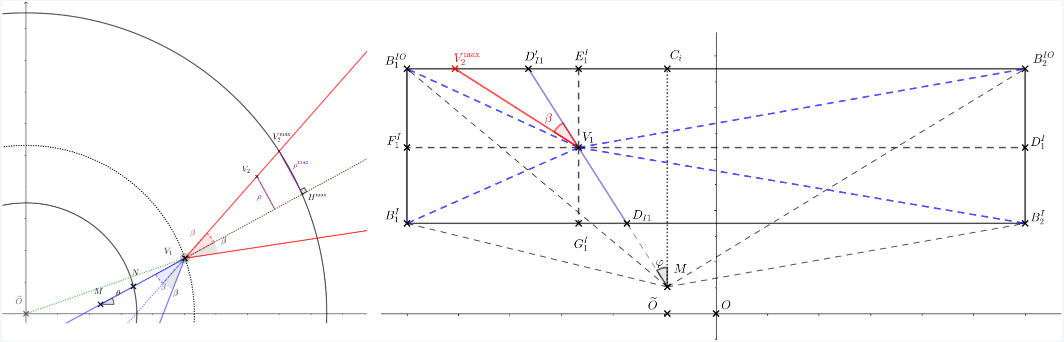

1γ case with incident energy E_0

Sensitivity calculation

Let M be an emission point of a E_0 photon belonging to the voxel j in the FOV:

$$s_{2\gamma}(M) := \int_{\theta=0}^{\pi}\int_{\varphi=0}^{\frac{\pi}{2}} p_i\left(\frac{1}{|\cos(\varphi)|}\left(\sqrt{R_{\text{out}}^{2\gamma}(\varphi, I1)^2 - \widetilde{O}\,P^2} - Q\right)\right) \times p_i\left(\frac{1}{|\cos(\varphi)|}\left(\sqrt{R_{\text{out}}^{2\gamma}(\varphi, J2)^2 - \widetilde{O}\,P^2} - Q\right)\right) \mathrm{d}\varphi$$

$$+ \int_{\varphi=-\frac{\pi}{2}}^{0} p_i\left(\frac{1}{|\cos(\varphi)|}\left(\sqrt{R_{\text{out}}^{2\gamma}(\varphi, I2)^2 - \widetilde{O}\,P^2} - Q\right)\right) \times p_i\left(\frac{1}{|\cos(\varphi)|}\left(\sqrt{R_{\text{out}}^{2\gamma}(\varphi, J1)^2 - \widetilde{O}\,P^2} - Q\right)\right) \mathrm{d}\varphi\mathrm{d}\theta$$

$$\widetilde{O}\,P := \sin(\theta)\,\widetilde{O}\,M, \quad Q := \sqrt{R_1^2 - \widetilde{O}\,P^2}.$$

$$s_{1\gamma}(M) := \int_{\theta=0}^{2\pi}\left[\int_{\varphi=0}^{\frac{\pi}{2}}\int_{v=R_{\text{in}}}^{R_{\text{out}}^{1\gamma}(\varphi, I1)} h(\varphi, \theta, v)\mathrm{d}v\mathrm{d}\varphi + \int_{\varphi=\frac{\pi}{2}}^{\pi}\int_{v=R_{\text{in}}}^{R_{\text{out}}^{1\gamma}(\varphi, J1)} h(\varphi, \theta, v)\mathrm{d}v\mathrm{d}\varphi\right.$$

$$\left. + \int_{\varphi=-\frac{\pi}{2}}^{0}\int_{v=R_{\text{in}}}^{R_{\text{out}}^{1\gamma}(\varphi, I2)} h(\varphi, \theta, v)\mathrm{d}v\mathrm{d}\varphi + \int_{\varphi=-\pi}^{-\frac{\pi}{2}}\int_{v=R_{\text{in}}}^{R_{\text{out}}^{1\gamma}(\varphi, J2)} h(\varphi, \theta, v)\mathrm{d}v\mathrm{d}\varphi\right]\mathrm{d}\theta$$

$$\text{with } h(\varphi, \theta, v) := f(\varphi, \theta, v) \times C(v, \theta, \varphi)$$

$$f(\varphi, \theta, v) := p_i\left(\frac{1}{|\cos(\varphi)|}\left(\sqrt{v^2 - \sin^2(\theta)\,\widetilde{O}\,M^2} - \sqrt{R_{\text{in}}^2 - \sin^2(\theta)\,\widetilde{O}\,M^2}\right)\right)$$

$$C(v, \theta, \varphi) := \int_{\beta=-\pi}^{\pi} K(\beta|E_0)\int_{\omega=0}^{2\pi}\int_{\rho=0}^{\rho_{\max}(v,\theta,\varphi,\beta,\omega)} p_i'\left(\|\overrightarrow{V_1V_2}\|_2\right)\mathrm{d}\beta\mathrm{d}\omega\mathrm{d}\rho$$